2010-0954

48th AIAA Aerospace Science Meeting, 4-7 January 2010, Orlando, Florida

# Analysis of the Reaction-Advection-Diffusion Spectrum of Laminar Premixed Flames

Ashraf N. Al-Khateeb*, Joseph M. Powers†

*University of Notre Dame, Notre Dame, Indiana, 46556-5637, USA*

**The dynamics of one-dimensional laminar premixed combustion in reactive mixtures described by a 1) simple one-species model, 2) simple two-species model, and 3) detailed chemical kinetics model with multicomponent transport in hydrogen–air is investigated. For each model 1) spatially homogeneous results are first obtained, followed by 2) time-independent, spatially inhomogeneous results, and ended by 3) a generalized eigenvalue analysis to calculate the spatially discretized systems' time scale spectrum. The results reveal that for spatially resolved structures, the systems' short wavelength modes are dominated by diffusion-based time scales, coarse wavelength modes are dominated by reaction-based time scales, and modes near a cross-over wavelength have time scales dictated by a combination of reaction and diffusion effects.**

## I. Introduction

SIMULATING chemically reactive flow involves solving a large set of partial differential equations (PDEs) which represents chemical species evolution coupled with the conservation of mass, momentum, and energy. For combustion problems which are inherently unsteady and spatially inhomogeneous, the dynamics are crucial. A common notion in combustion theory is that chemical dynamics are somehow segregated from the dynamics of advection and diffusion; this notion is especially prevalent in discussion of so-called operator splitting strategies for numerical simulation of combustion events. In reality, unsteady, spatially inhomogeneous combustion is better viewed as an event in which reaction, advection, and diffusion time scales are often fully coupled.

For accurate modeling, the interplay between chemistry and transport needs to be captured. One way to gain a better understanding of the coupling between transport and chemistry can be achieved via conducting a spectral analysis of a plane laminar flame structure. It is important in a spectral analysis to guarantee that all length scales in the underlying steady structure problem have been brought into simultaneous focus. In recent studies,[1,2] it has been shown that the finest length scale for an atmospheric-pressure laminar premixed flame is typically on the order of $10^{-4}$ $cm$.

This work will consider linear analysis of three one-dimensional unsteady models of increasing complexity. For each problem, we will identify 1) the time scales associated with the spatially homogeneous version of the model, 2) the length scales associated with the steady state version of the model, and 3) the time scales associated with each Fourier mode of varying wavelength for the full unsteady spatially inhomogeneous model. In the first problem, we consider a simple model with one species subjected to reaction, advection, and diffusion. In the second problem, we consider a slightly more complex model in which two uncoupled species react at two disparate rates and diffuse at the same rate. In the third we consider a premixed mixture of $N$ calorically imperfect ideal gases that react and diffuse at $N$ widely disparate rates. For this problem, we specifically consider a $N = 9$ species model of hydrogen–air combustion.

*Ph.D. Candidate, Department of Aerospace and Mechanical Engineering, AIAA Student Member, aalkhate@gmail.com.

†Professor, Department of Aerospace and Mechanical Engineering, AIAA Associate Fellow, powers@nd.edu.

## II. Simple one species problem

Consider a linear reaction-advection-diffusion PDE, initial, and boundary conditions,

$$\frac{\partial \psi(x,t)}{\partial t} + u\frac{\partial \psi(x,t)}{\partial x} = D\frac{\partial^2 \psi(x,t)}{\partial x^2} - a\psi(x,t), \qquad \psi(x,0) = \psi_u, \quad \psi(0,t) = \psi_u, \quad \left.\frac{\partial \psi}{\partial x}\right|_{x=L} = 0. \tag{1}$$

where the independent variables $t > 0$ and $x \in [0, L]$ represent the time and distance coordinates, respectively. Here, $\psi(x,t)$ is a general scaler; $u > 0$ is a constant wave speed for a right running wave; $D > 0$ is a diffusion coefficient, and $a > 0$ is the consumption rate constant.

### II.A. Time scale spectrum

The spatially homogenous version of Eq. (1) is

$$\frac{d\psi(t)}{dt} = -a\psi(t), \qquad \psi(0) = \psi_u. \tag{2}$$

This has solution

$$\psi(t) = \psi_u \exp\left(-at\right). \tag{3}$$

The time scale $\tau$ over which $\psi$ evolves is $\tau = 1/a$; there is only one time scale in this spectrum. To capture these dynamics in a numerical simulation, it is necessary to employ $\Delta t < 1/a$. Since there is only one time scale, this formulation of the system is not temporally stiff.

### II.B. Length scale spectrum

A simple means to determine an upper bound for the required grid resolution is to solve for the steady structure $\psi_s(x)$, which is governed by

$$u\frac{d\psi_s(x)}{dx} = D\frac{d^2\psi_s(x)}{dx^2} - a\psi_s(x), \qquad \psi_s(0) = \psi_u, \quad \left.\frac{d\psi_s}{dx}\right|_{x=L} = 0. \tag{4}$$

The solution of Eq. (4) is

$$\psi_s(x) = \psi_u \left( \frac{\exp(\mu_1 x) - \exp(\mu_2 x)}{1 - \frac{\mu_1}{\mu_2}\exp(L(\mu_1 - \mu_2))} + \exp(\mu_2 x) \right), \tag{5}$$

where

$$\mu_1 = \frac{u}{2D}\left(1 + \sqrt{1 + \frac{4aD}{u^2}}\right), \qquad \mu_2 = \frac{u}{2D}\left(1 - \sqrt{1 + \frac{4aD}{u^2}}\right). \tag{6}$$

Because of the imposed positivity of $u$, $D$, and $a$, we see that $\mu_1 > 0$ and $\mu_2 < 0$.

There are two length scales in this discrete spatial spectrum, $\ell_1 = |1/\mu_1|$, $\ell_2 = |1/\mu_2|$, twice the number in the time scale spectrum found earlier. The scale $\ell_1$ becomes irrelevant in the limit as $L \to \infty$. In that limit, recalling that $x \in [0, \infty)$, the steady solution becomes

$$\psi_s(x) = \psi_u \exp(\mu_2 x). \tag{7}$$

Let us examine Eq. (6) in the limit when reaction dominates advection and diffusion, $a >> u^2/D$. In this limit Eq. (6) reduces to $\mu_{1,2} \sim \pm\sqrt{a/D}$, and thus

$$\ell_1 = \ell_2 = \ell = \left|\frac{1}{\mu_{1,2}}\right| = \sqrt{\frac{D}{a}}. \tag{8}$$

We take the spatial stiffness $\mathcal{S}_x$ as the ratio of the largest to the smallest length scale. Since both are the same, the spatial stiffness here is unity, $\mathcal{S}_x = 1$, *i.e.* the system is not spatially stiff. The length scale $\ell$ provides an upper bound for the required numerical resolution, $\Delta x \leq \ell$, in order for any numerical calculation to remain faithful to the underlying mathematics, which itself reflects the physics of coupled reaction-advection-diffusion, and to bring the numerical solution of Eq. (1) into the convergence domain.

## II.C. Spatio-temporal spectrum

### *II.C.1. Continuous spectrum*

In the limit as $L \to \infty$, it is possible to find a simple analytic expression for the continuous spectrum of time scales $\tau$ associated with a particular Fourier mode of wavenumber $k$. A Fourier mode with wavenumber $k$ has wavelength $\lambda = 2\pi/k$. We ignore here boundary conditions and assume a solution of the form

$$\psi(x,t) = \Psi(t)e^{\mathbb{i}kx}, \tag{9}$$

where $\Psi(t)$ is the time-dependent amplitude of the chosen Fourier mode. Substituting this into Eq. (1) gives the ordinary differential equation (ODE):

$$\frac{d\Psi(t)}{dt} = -\left(\mathbb{i}ku + Dk^2 + a\right)\Psi(t). \tag{10}$$

This has a solution of the form

$$\Psi(t) = C\exp\left(-(\mathbb{i}ku + Dk^2 + a)t\right), \tag{11}$$

where $C$ is an arbitrary constant. The continuous time scale spectrum thus is given by

$$\tau = \frac{1}{a + \mathbb{i}uk + Dk^2}, \qquad 0 < k \in \mathbb{R}. \tag{12}$$

From Eq. (12), it is clear that for small wavenumbers, *i.e.* long wavelengths, the time scales will be dominated by reaction:

$$\lim_{k\to 0}\tau = \lim_{\lambda\to\infty}\tau = \frac{1}{a}. \tag{13}$$

However, for large wavenumber (small wavelength) the time scales are dominated by diffusion:

$$\lim_{k\to\infty}\tau = \lim_{\lambda\to 0}\tau = \frac{1}{Dk^2} = \frac{1}{4\pi^2}\frac{\lambda^2}{D}. \tag{14}$$

Advection does not play a role in determining the limiting values of the time scale spectrum. We take the temporal stiffness $\mathcal{S}_t$ as the ratio of the largest to the smallest time scale. Here we have

$$\mathcal{S}_t = \frac{1/a}{\lambda^2/(4\pi^2 D)}, \tag{15}$$

and we see as the wavelength approaches zero, the stiffness becomes infinite.

From Eq. (12) we see that a balance between reaction and diffusion exists for wavenumber $k = \sqrt{a/D}$. In terms of wavelength and recalling Eq. (8), we see the balance at

$$\frac{\lambda}{2\pi} = \sqrt{\frac{D}{a}} = \ell, \tag{16}$$

where $\ell = 1/k$ is proportional to the wavelength.

Let us now study how the magnitude of $\tau$ varies with wavelength as predicted by Eq. (12). We find by expansion that the magnitude of the complex $\tau$ is given by

$$|\tau| = \left(\left(a + \frac{D}{\left(\frac{\lambda}{2\pi}\right)^2}\right)^2 + \frac{u^2}{\left(\frac{\lambda}{2\pi}\right)^2}\right)^{-1/2}. \tag{17}$$

Additional insight is gained by examining how $|\tau|$ behaves in the long wavelength limit. Taylor expansion of Eq. (17) in this limit reveals that

$$|\tau| = \frac{1}{a}\left(1 - \frac{D}{a\left(\frac{\lambda}{2\pi}\right)^2} - \frac{u^2}{2a^2\left(\frac{\lambda}{2\pi}\right)^2}\right) + \mathcal{O}\left(\frac{1}{\lambda^4}\right). \tag{18}$$

So in the large $\lambda$ limit, $|\tau|$ is dominated by reaction effects, and we see that advection and diffusion both lower its magnitude.

We examine the behavior of the system quantitatively by choosing numerical values of $a = 10^8\ 1/s$, $D = 10^1\ cm^2/s$, $u = 10^2\ cm/s$. These values are somewhat similar to those for the fastest reaction in a hydrogen–air flame at atmospheric pressure. For these values, we find the estimate from Eq. (8) for the length scale where reaction balances diffusion as $\ell = \lambda/(2\pi) = 3.2 \times 10^{-4}\ cm$. A plot of $|\tau|$ versus $\ell = \lambda/(2\pi)$ from Eq. (17) is given in Fig. (1). For long wavelengths, the time scales are determined by reaction; for fine wavelengths, the time scale's falloff is dictated by diffusion, and our simple formula for the critical $\ell$ predicts the transition well. Lastly, for small $\lambda$, it is seen that a one decade decrease in $\lambda$ induces a two decade decrease in $|\tau|$, consistent with the prediction of Eq. (14) of $\lim_{\lambda\to 0} \ln \tau \sim 2 \ln \lambda - \ln(4\pi^2 D)$.

### *II.C.2. Discrete spectrum*

For finite $L$, Eq. (1) possesses a discrete spectrum of time scales, not given here, which reduces to the continuous spectrum in the limit of large $L$. To find this, one would use separation of variables to solve the initial-boundary value problem.

### *II.C.3. Spatially discretized spectrum*

Original boundary conditions. We next approximate the time scale spectrum of Eq. (1) following discrete approximation of the spatial derivative operators. We do this for illustrative purposes, as the same technique will be used for the more complicated problem of detailed chemical kinetics later. To this end, Eq. (1) is spatially discretized $\psi(x,t) \to \psi_i(t)$ using a second order central difference scheme. After rearrangement of Eq. (1) and application of both boundary conditions, we find the system of Differential Algebraic Equations (DAEs):

$$\frac{d\psi_1}{dt} = 0, \tag{19a}$$

$$\frac{d\psi_i}{dt} = \psi_{i+1}\left(\frac{D}{\Delta x^2} - \frac{u}{2\Delta x}\right) - \psi_i\left(a + \frac{2D}{\Delta x^2}\right) + \psi_{i-1}\left(\frac{D}{\Delta x^2} + \frac{u}{2\Delta x}\right), \quad i = 2, \ldots, \mathcal{N}-1, \tag{19b}$$

$$0 = 3\psi_{\mathcal{N}} - 4\psi_{\mathcal{N}-1} + \psi_{\mathcal{N}-2} \tag{19c}$$

where $\Delta x > 0$ and $\mathcal{N} > 3$ is the total number of the spatial points. Equation (19b) takes a general compact form of

$$\mathbf{A} \cdot \frac{d\boldsymbol{\psi}}{dt} = \mathbf{B} \cdot \boldsymbol{\psi}. \tag{20}$$

Here $\mathbf{A}$ is a singular matrix. If we assume $\boldsymbol{\psi}$ is approximated by $\boldsymbol{\upsilon}\exp(\mu t)$, Eq. (20) reduces to

$$(\mu\mathbf{A} - \mathbf{B}) \cdot \boldsymbol{\upsilon} = \mathbf{0}. \tag{21}$$

This is a generalized eigenvalue problem, with generalized eigenvalues $\mu$ and generalized eigenvectors $\boldsymbol{\upsilon}$, which approximate the eigenfunctions of the continuous spatial derivative operator. Both of these can easily be studied numerically.

Dirichlet boundary condition modification. Additional insights can be drawn by a slight modification of the $x = L$ boundary condition to $\psi(L,t) = \psi_u$. As a result, Eq. (19b) becomes a complete system, as the values for $\psi_1$ and $\psi_{\mathcal{N}}$ are now known. The system takes can be written in the form

$$\frac{d\boldsymbol{\psi}}{dt} = \mathbf{B} \cdot \boldsymbol{\psi} + \mathbf{C}, \tag{22}$$

where $\mathbf{C}$ is a constant vector, and $\mathbf{B}$ is a tri-diagonal constant matrix. The time scale spectrum of Eq. (22) is given by the reciprocal of each of matrix $\mathbf{B}$'s eigenvalues. Since $\mathbf{B}$ is a tridiagonal constant matrix, its eigenvalues can be calculated analytically using a known formula.[3] They are, after rearrangement,

$$\mu_j = -a - \frac{2D}{\Delta x^2}\left(1 - \sqrt{1 - \frac{u^2\Delta x^2}{4D^2}}\cos\left(\frac{j\pi}{\mathcal{N}-1}\right)\right), \quad j = 1, \ldots, \mathcal{N}-2. \tag{23}$$

Thus, the time scales are

$$\tau_j = \frac{1}{a + \frac{2D}{\Delta x^2}\left(1 - \sqrt{1 - \frac{u^2\Delta x^2}{4D^2}}\cos\left(\frac{j\pi}{\mathcal{N}-1}\right)\right)}, \quad j = 1, \ldots, \mathcal{N}-2. \tag{24}$$

From Eq. (24), it is clear that for large $\Delta x$, the time scales will be dominated by reaction, $\lim_{\Delta x\to\infty} \tau_j \to 1/a$. Consequently, to capture these reaction dynamics, it is necessary to employ $\Delta t \leq 1/a$. We can capture the first effects of advection and diffusion by studying Eq. (24) in the limits of large $\mathcal{N}$ and fast reaction ($a >> D/L^2,\ a >> u^2/D$) and focusing on the fundamental mode, $j = 1$. In this case, Taylor series expansion reveals that

$$\tau_1 \sim \frac{1}{a}\left(1 - \frac{D}{a(L/\pi)^2} - \frac{1}{4}\frac{u^2}{aD}\right). \tag{25}$$

Thus, advection and diffusion induce a lowering of the time scale of the fundamental mode, and these dynamics are based on the physics not the discretization.

On the other hand, for small $\Delta x$ the time scales become dominated by diffusion,

$$\lim_{\Delta x\to 0} \tau_j \to \frac{\Delta x^2}{4D}. \tag{26}$$

So, the time step to capture diffusion dynamics is $\Delta t \leq \Delta x^2/(4D)$. Now, in order to resolve the spatial structure, the upper bound for the required spatial resolution given by Eq. (8) must at least be employed, $\Delta x = \sqrt{D/a}$. By substituting that into Eq. (26), it is clear that the fastest time scale in the minimally resolved solution is $\tau = 1/(4a)$. This is a consequence of the system identifying a natural length scale where reaction balances diffusion. The temporal stiffness ratio here is

$$\mathcal{S}_t = \frac{1/a}{\Delta x^2/(4D)}, \tag{27}$$

and becomes ever-greater as $\Delta x$ is decreased. Lastly, it is clear that advection is not a major player in determining the system's finest time scale.

## III. Simple two species problem

In this model problem, an uncoupled reaction-diffusion system of PDEs that exhibits chemical stiffness is considered; the advection term is excluded. We take

$$\frac{\partial \psi_1}{\partial t} = D\frac{\partial^2 \psi_1}{\partial x^2} - a_1\psi_1, \tag{28}$$

$$\frac{\partial \psi_2}{\partial t} = D\frac{\partial^2 \psi_2}{\partial x^2} - a_2\psi_2, \tag{29}$$

$$\psi_1(0,t) = \psi_{1u}, \quad \psi_2(0,t) = \psi_{2u}, \tag{30}$$

$$\frac{\partial \psi_1}{\partial x}(L,t) = 0, \quad \frac{\partial \psi_2}{\partial x}(L,t) = 0, \tag{31}$$

$$\psi_1(x,0) = \psi_{1u}, \quad \psi_2(x,0) = \psi_{2u}. \tag{32}$$

where $x \in [0, L], a_1 >> a_2 > 0$, and $D > 0$. The chemical stiffness is a consequence of $a_1 >> a_2$. Similar to the previous example, we will see that in addition to chemical stiffness that diffusion induces additional stiffness, which can be even more demanding than chemical stiffness.

### III.A. Time scale spectrum

Here, the spatially homogenous version of this system of PDEs, Eqs. (28)–(29), is given by

$$\frac{d\psi_1}{dt} = -a_1\psi_1, \quad \psi_1(0) = \psi_{1u} \tag{33}$$

$$\frac{d\psi_2}{dt} = -a_2\psi_2, \quad \psi_2(0) = \psi_{2u}, \tag{34}$$

The solution is

$$\psi_1(t) = \psi_{1u}\exp(-a_1 t), \qquad \psi_2(t) = \psi_{2u}\exp(-a_2 t). \tag{35}$$

The system has two time scales in its spectrum which are $\tau_1 = 1/a_1, \tau_2 = 1/a_2$; the temporal stiffness is $\mathcal{S}_t = a_1/a_2$, and the fastest time scale over which the system evolves is $\tau_1 = 1/a_1$. Thus, to capture the physical dynamics in a numerical simulation $\Delta t < 1/a_1$ needs to be employed.

### III.B. Length scale spectrum

To determine an upper bound for the required grid resolution, we solve for the steady structure $\psi_{is}(x), i = 1, 2$ of Eqs. (28)-(29), which is governed by

$$D\frac{d^2\psi_{1s}(x)}{dx^2} = a_1\psi_{1s}(x), \tag{36}$$

$$D\frac{d^2\psi_{2s}(x)}{dx^2} = a_2\psi_{2s}(x). \tag{37}$$

We take the boundary conditions to be

$$x = 0: \qquad \psi_1 = \psi_{1u}, \quad \psi_2 = \psi_{2u}, \tag{38}$$

$$x = L: \qquad \frac{d\psi_1}{dx} = \frac{d\psi_2}{dx} = 0. \tag{39}$$

Assuming solutions of the form $\psi_{is}(x) = C\exp(\mu x)$ leads to two characteristic polynomials of the form $D\mu^2 - a_i = 0$. These yield four roots $\mu = \pm\sqrt{a_i/D}$, $i = 1, 2$. This induces four length scales; note this is twice as many as the two time scales associated with the spatially homogeneous version of Eqs. (28)-(29). The associated length scales, two of which are degenerate, are $\ell = \sqrt{D/a_i}$, $i = 1, 2$. So the system exhibits a spatial stiffness of $\mathcal{S}_x = \sqrt{a_1/a_2}$.

The steady solution is given by

$$\psi_{1s}(x) = \frac{\psi_{1u}}{\cosh\left(\sqrt{\frac{a_1}{D}}L\right)}\cosh\left(\sqrt{\frac{a_1}{D}}(L-x)\right), \tag{40}$$

$$\psi_{2s}(x) = \frac{\psi_{2u}}{\cosh\left(\sqrt{\frac{a_2}{D}}L\right)}\cosh\left(\sqrt{\frac{a_2}{D}}(L-x)\right), \tag{41}$$

Because $a_1 >> a_2$, the smallest physical length scale that has to be captured is

$$\ell = \sqrt{\frac{D}{a_1}}. \tag{42}$$

### III.C. Spatio-temporal spectrum

#### *III.C.1. Continuous spectrum*

Similar to the one species model, if we take $L \to \infty$ and ignore the boundary conditions, it is possible to find a simple analytic expression for the continuous spectrum of time scales associated with each particular Fourier mode. The details of the analysis are similar to that previously given. We assume $\psi_i(x,t) = \Psi_i(t)\exp(\mathbf{i}kx)$, which leads to

$$\tau_i = \frac{1}{a_i + Dk^2}, \qquad 0 < k \in \mathbb{R}. \tag{43}$$

We then see that $\lim_{k\to 0}\tau_i = \lim_{\lambda\to\infty}\tau_i = 1/a_i$, and $\lim_{k\to\infty}\tau_i = \lim_{\lambda\to 0}\tau_i = 1/(Dk^2) = \lambda^2/(4\pi^2 D)$.

#### *III.C.2. Discrete spectrum*

Now consider finite $L$ and re-employ the appropriate boundary conditions. It can be shown using separation of variables that the solution of Eqs. (28)–(29), is given by

$$\psi_i(t,x) = \psi_{is}(x) + \sum_{\kappa=1}^{\infty} A_\kappa \exp\left(-\left(a_i + \frac{(2\kappa-1)^2\pi^2 D}{4L^2}\right)t\right)\sin\left(\frac{(2\kappa-1)\pi}{2L}x\right), \quad i = 1, 2, \tag{44}$$

where $A_\kappa$ are constants that can be determined by a Fourier decomposition of the initial conditions. Consequently, the analytical time scale spectrum of this system is given by

$$\tau_i = \frac{1}{a_i + D\left(\frac{(2\kappa-1)\pi}{2L}\right)^2}, \qquad i = 1, 2, \quad \kappa = 1, 2, \ldots, \infty. \tag{45}$$

Because we chose a finite spatial domain, the spectrum is discrete.

### *III.C.3. Spatially discretized spectrum*

To illustrate the numerical method which will be used for realistic chemistry, we numerically approximate the time scale spectrum using a discrete representation of the differential operators. Thus, the eigenvalue spectrum of Eqs. (28)–(29) is calculated. First, Eqs. (28)–(29) are spatially discretized using second order central differences. The resulting system of ODEs is written in a compact form as

$$\mathbf{A} \cdot \frac{d\mathbf{z}}{dt} = \mathbf{B} \cdot \mathbf{z}, \tag{46}$$

where $\mathbf{A}$ and $\mathbf{B}$ are constant matrices of size $4\mathcal{N} \times 4\mathcal{N}$, and $\mathbf{z}$ is the set of dependent variables,

$$\mathbf{A} = \left[\begin{array}{c|c} \mathbf{I}_{2\mathcal{N}\times 2\mathcal{N}} & \mathbf{0}_{2\mathcal{N}\times 2\mathcal{N}} \\ \hline \mathbf{0}_{2\mathcal{N}\times 2\mathcal{N}} & \mathbf{0}_{2\mathcal{N}\times 2\mathcal{N}} \end{array}\right], \tag{47}$$

$$\mathbf{B} = \left[\begin{array}{c|c|c|c} a_1\mathbf{I}_{\mathcal{N}\times\mathcal{N}} & \mathbf{0}_{\mathcal{N}\times\mathcal{N}} & \boldsymbol{\Delta}_{\mathcal{N}\times\mathcal{N}} & \mathbf{0}_{\mathcal{N}\times\mathcal{N}} \\ \hline \mathbf{0}_{\mathcal{N}\times\mathcal{N}} & a_2\mathbf{I}_{\mathcal{N}\times\mathcal{N}} & \mathbf{0}_{\mathcal{N}\times\mathcal{N}} & \boldsymbol{\Delta}_{\mathcal{N}\times\mathcal{N}} \\ \hline \boldsymbol{\mathfrak{D}}_{\mathcal{N}\times\mathcal{N}} & \mathbf{0}_{\mathcal{N}\times\mathcal{N}} & \multicolumn{2}{c}{\multirow{2}{*}{$\mathbf{I}_{2\mathcal{N}\times 2\mathcal{N}}$}} \\ \cline{1-2} \mathbf{0}_{\mathcal{N}\times\mathcal{N}} & \boldsymbol{\mathfrak{D}}_{\mathcal{N}\times\mathcal{N}} & & \end{array}\right], \tag{48}$$

$$\mathbf{z} = \begin{bmatrix} \psi_{1i} \\ \psi_{2i} \\ \frac{d\psi_{1i}}{dx} \\ \frac{d\psi_{2i}}{dx} \end{bmatrix}, \qquad i = 1, \ldots, \mathcal{N}, \tag{49}$$

$$\tag{50}$$

where

$$\boldsymbol{\mathfrak{D}} = \begin{bmatrix} \frac{-3D}{2\Delta x} & \frac{2D}{\Delta x} & \frac{-D}{2\Delta x} & & \\ \frac{-D}{2\Delta x} & 0 & \frac{D}{2\Delta x} & & \mathbf{0} \\ & \ddots & \ddots & \ddots & \\ & & \frac{-D}{2\Delta x} & 0 & \frac{D}{2\Delta x} \\ \mathbf{0} & & 0 & 0 & 0 \end{bmatrix}, \tag{51}$$

$$\boldsymbol{\Delta} = \begin{bmatrix} 0 & 0 & 0 & & \\ \frac{-1}{2\Delta x} & 0 & \frac{1}{2\Delta x} & & \mathbf{0} \\ & \ddots & \ddots & \ddots & \\ & & \frac{-1}{2\Delta x} & 0 & \frac{1}{2\Delta x} \\ \mathbf{0} & & \frac{-1}{2\Delta x} & \frac{2}{\Delta x} & \frac{-3}{2\Delta x} \end{bmatrix}. \tag{52}$$

Second, the eigenvalues of Eq. (46) are calculated. Since $\mathbf{A}$ is singular, standard eigenvalue analysis is not applicable. Instead, the generalized eigenvalues and the associated generalized eigenvectors, (*i.e.* discrete approximations of the continuous eigenfunctions, which are normal modes), of this dynamical system are calculated.[3] The system's time scales are the reciprocals of its generalized eigenvlaues.

For a system with $a_1 = 10^4\ 1/s, a_2 = 10^2\ 1/s, D = 10^1\ cm^2/s$ and a length $L = 10^1\ cm$, the system's time scale spectrum is presented in Fig. 2. Here, for the numerical results, the modified wavelength $\widehat{\lambda}$ has been defined based on the number of zero crossings (*i.e.* normal mode nodes) $\mathfrak{n}$, such that

$$\widehat{\lambda} = \frac{4L}{2\mathfrak{n} - 1}, \qquad \mathfrak{n} = 1, 2, \ldots \tag{53}$$

We see that the associated length scale $\ell = \widehat{\lambda}/(2\pi)$ is

$$\ell = \frac{2L}{(2\mathfrak{n}-1)\pi}, \qquad \mathfrak{n} = 1, 2, \ldots. \tag{54}$$

This can be directly compared with the length scale associated with the sine wave of Eq. (44), which is $\ell_\kappa = 2L/((2\kappa-1)\pi),\ \kappa = 1, 2, \ldots$.

Figure 2 shows that the numerically estimated time scales associated with large wavelength modes agree well with the ones predicted analytically; numerical error becomes higher as the wavelength decreases. Because of the difficulty in calculating the generalized eigenvalues and eigenvectors of large systems, only a small window of about three decades of wavelength is shown in Fig. 2.

By focusing only on the fundamental mode and varying $L$, a clearer understanding can be realized. In Fig. 3, the system's time scales associated with the fundamental modes, *i.e.* eigenfunctions with $\mathfrak{n} = 1$, are tracked as we vary $L$. Because for $\mathfrak{n} = 1$, $\widehat{\lambda} = 2L$ from Eq. (53), we have $\widehat{\lambda}/(2\pi) = L/\pi$, and we use this for the abscissa. Here, turning points are seen near $L/\pi \sim 3 \times 10^{-1}$ $cm$ and $L/\pi \sim 3 \times 10^{-2}$ $cm$ and represent the length scales where diffusion starts to balance reaction. For this system, one independently predicts from Eq. (42) that the reaction-diffusion balance for the fastest reaction exists at $\ell_1 = 3.2 \times 10^{-2}$ $cm$. For the slowest reaction, one would comparably predict the balance to exist at $\ell_2 = 3.2 \times 10^{-1}$ $cm$. Moreover, short domain lengths have fast time scales which are dominated by diffusion, and long domain lengths have time scales which are reaction-dominated. Furthermore, the effect of adopting identical diffusion coefficients for each species evolution equation is realized in the diffusion-dominated region; here the two time scales associated with the fundamental modes are identical.

## IV. Laminar Premixed Flames

The one-dimensional laminar premixed mixture of $N$ molecular species composed of $\mathsf{L}$ atomic elements which undergoes $J$ reversible reactions is modeled by the reactive Navier-Stokes equations. By neglecting body forces and adopting the low-Mach number assumption, which is reasonable for weak deflagration,[4] the governing equations can be written as

$$\frac{\partial \rho}{\partial t} + \frac{\partial}{\partial x}(\rho u) = 0, \tag{55}$$

$$\frac{\partial}{\partial t}(\rho h) + \frac{\partial}{\partial x}(\rho u h + \mathrm{J}^q) = 0, \tag{56}$$

$$\frac{\partial}{\partial t}(\rho Y_i) + \frac{\partial}{\partial x}(\rho u Y_i + \mathrm{J}_i^m) = \dot{\omega}_i \bar{m}_i, \quad i = 1, \ldots, N-1, \tag{57}$$

where the independent variables are the spatial coordinate $x$ and the time $t$. In Eqs. (56)–(57), $u$ is the mixture velocity, $\rho$ is the mass density, $h$ is the mixture specific enthalpy, $\mathrm{J}^q$ is total heat flux, and for the $i^{th}$ species, $\bar{m}_i, Y_i, \mathrm{J}_i^m$ and $\dot{\omega}_i$ are the molecular mass, the mass fraction, the diffusive mass flux, and the molar production rate per unit volume, respectively.

By neglecting the thermal diffusion effects, the constitutive relations for diffusive mass fluxes and heat flux are

$$\mathrm{J}_i^m = \frac{\rho \bar{m}_i}{\bar{m}} \sum_{\substack{j=1 \\ j \neq i}}^{N} \frac{D_{ij} Y_j}{X_j} \frac{\partial X_j}{\partial x}, \quad i = 1, \ldots, N, \tag{58}$$

$$\mathrm{J}^q = \mathrm{q} + \sum_{i=1}^{N} \mathrm{J}_i^m h_i, \tag{59}$$

where

$$\mathrm{q} = -\mathsf{k} \frac{\partial T}{\partial x}. \tag{60}$$

Here, $T$ is the temperature, q is the Fourier heat flux, $D_{ij}$ is the multi-compenent diffusion coefficient, $\mathsf{k}$ is the mixture thermal conductivity, and for the $i^{th}$ species, $X_i, h_i$ are the mole fraction and the specific

enthalpy, respectively. To complete the system, the following set of relations is adopted,

$$
\begin{aligned}
p &= \rho\bar{\Re}T\sum_{i=1}^{N}\frac{Y_i}{\bar{m}_i}, && \text{(61a)}\\
\dot{\omega}_i &= \sum_{j=1}^{J}\nu_{ij}A_j\ T^{\beta_j}\ \exp\left(\frac{-\bar{E}_j}{\bar{\Re}T}\right)\left(\prod_{i=1}^{N}(\bar{\rho}_i)^{\nu'_{ij}} - \frac{1}{K_j^c}\prod_{i=1}^{N}(\bar{\rho}_i)^{\nu''_{ij}}\right), \quad i=1,\ldots,N, && \text{(61b)}\\
K_j^c &= \left(\frac{p^{ref}}{\bar{\Re}T}\right)^{\sum_{i=1}^{N}\nu_{ij}}\exp\left(-\frac{\sum_{i=1}^{N}\bar{\mu}_i^o\nu_{ij}}{\bar{\Re}T}\right), \quad j=1,\ldots,J, && \text{(61c)}\\
h_i &= h_i^f + \int_{T^{ref}}^{T} c_{pi}(\tilde{T})d\tilde{T}, \quad i=1,\ldots,N, && \text{(61d)}\\
s_i^o &= s_i^f + \int_{T^{ref}}^{T}\frac{c_{pi}}{\tilde{T}}d\tilde{T}, \quad i=1,\ldots,N, && \text{(61e)}\\
\bar{\mu}_i^o &= \bar{m}_i\left(h_i - Ts_i^o\right), \quad i=1,\ldots,N, && \text{(61f)}\\
h &= \sum_{i=1}^{N}Y_ih_i, && \text{(61g)}\\
\bar{m} &= \sum_{i=1}^{N}X_i\bar{m}_i, && \text{(61h)}\\
X_i &= \frac{\bar{m}}{\bar{m}_i}Y_i, \quad i=1,\ldots,N, && \text{(61i)}\\
\bar{\rho}_i &= \frac{\rho Y_i}{\bar{m}_i}, \quad i=1,\ldots,N, && \text{(61j)}\\
\nu_{ij} &= \nu''_{ij} - \nu'_{ij}, \quad i=1,\ldots,N, \quad j=1,\ldots,J, && \text{(61k)}\\
0 &= \sum_{i=1}^{N}\phi_{li}\nu_{ij}, \quad j=1,\ldots,J, \quad l=1,\ldots,\mathsf{L}, && \text{(61l)}\\
1 &= \sum_{i=1}^{N}Y_i, && \text{(61m)}\\
0 &= \sum_{i=1}^{N}\mathrm{J}_i^m, && \text{(61n)}
\end{aligned}
$$

In Eqs. (61), $p$ is the pressure, $\bar{m}$ is the mixture-average molecular mass, $K_j^c$ denotes the equilibrium constant for the $j^{th}$ reaction, $\phi_{li}$ the element index of species $i$, which gives the number of moles of element $l$ in species $i$, and for the $i^{th}$ specie, $\bar{\rho}_i, c_{pi}, s_i^o$, and $\bar{\mu}_i^o$, which are the concentration (*i.e.* molar density), mass-based specific heat at constant pressure, mass-based specific entropy at standard pressure, and molar-basis specific chemical potential, respectively. The constant parameters are the universal gas constant $\bar{\Re} = 8.314\times10^7\ erg/mole/K$ is the universal gas constant, $p^{ref} = 1\ atm$ the reference pressure, and $T^{ref} = 298\ K$ the reference temperature. Also, for each reaction from $j = 1,\ldots,J$, there are $A_j, \beta_j, \bar{E}_j, \nu''_{ij}, \nu'_{ij}$, and $\nu_{ij}$ which represent the collision frequency factor, the temperature-dependency exponent, the activation energy, the stoichiometric coefficients of species $i$ denoting the number of moles of products, reactants, and the net stoichiometric coefficient, respectively.

In this work, the employed kinetic mechanism is extracted from Miller *et al.*[5] This mechanism consists of $J = 19$ reversible reactions involving $N = 9$ species, see Table 1. In this mechanism, the reactant species are $H_2, O_2, H, O, OH, HO_2, H_2O_2$, and $H_2O$. The inert diluent for the mixture is $N_2$.

### IV.A. Time scale spectrum

First, we consider unsteady spatially homogeneous systems. Thus, the governing equations, extracted from Eqs. (55)–(57), are the following set of ODEs:

$$\frac{dh}{dt} = 0, \tag{62}$$

$$\frac{dY_i}{dt} = \frac{\dot{\omega}_i \bar{m}_i}{\rho}, \qquad i = 1, \ldots, N, \tag{63}$$

where $\rho$ is governed by the thermal equation of state (61a).

To calculate the time scale spectrum over which the system evolves, an eigenvalue analysis is performed.[6] The set of ODEs are lineraized at each time step about the local solution state, and the temporally local Jacobian matrix $\mathbf{J}$ is calculated. The local time scales $\tau_i$ over which the system evolves are given by the reciprocal of the real parts of the local $\mathbf{J}$'s eigenvalues; $\tau_i = 1/\left|Re(\mu_i)\right|$. Furthermore, the ratio between the largest and the smallest time scales identifies the system's temporal stiffness, $\mathcal{S}_t$.

Here, a stoichiometric atmospheric–pressure premixed mixture is considered, where the initial molar ratio is given by $2H_2 + O_2 + 3.76N_2$. The system is adiabatic, isobaric, and initially at $T^* = 1000\ K$. The evolution of species mass fractions and the time scales over which the system evolves are presented in Figs. 4–5.

In Fig. 4, at $t \approx 10^{-7}\ s$ the species growth rates change slightly, which indicates that significant dissociation reactions are induced. For $10^{-6} < t < 10^{-4}\ s$, the minor species continue to increase rapidly with different growth rates. On the other hand, the major species $H_2, O_2$, and $N_2$ have essentially constant concentrations. Just past $t \approx 10^{-4}\ s$ all the species undergo significant change, and the radicals' mass fractions reach their maximum values. At $t \approx 3 \times 10^{-4}\ s$, an exothermic recombination of radicals commences forming the predominant product $H_2O$, which continues up to $t \approx 10^{-3}\ s$, after which the system approaches the equilibrium state.

The time scales over which the system evolves are presented in Fig. 5. There are six time scales in the spectrum. Because our reaction mechanism has $N = 9$ species with $\mathsf{L} = 3$ elements being conserved, we find $N - \mathsf{L} = 6$ independent modes. The multi-scale nature of this problem is clearly seen. Near equilibrium the slowest time scale is $\mathcal{O}(10^{-4}\ s)$, and the fastest time scale is $\mathcal{O}\left(10^{-8}\ s\right)$, giving rise to $\mathcal{S}_t \sim \mathcal{O}(10^4)$. The fastest time scale is consistent with the time scale over which minor species evolve.

### IV.B. Length scale spectrum

For the steady planar flame, the following set of equations, which commonly appears in the literature[7–9] and can be easily extracted from Eqs. (55)–(57), is used

$$\frac{d}{dx}(\rho u) = 0, \tag{64}$$

$$\rho u c_p \frac{dT}{dx} + \frac{d\mathrm{q}}{dx} = -\sum_{i=1}^{N} \left( \mathrm{J}_i^m \frac{dh_i}{dx} + \dot{\omega}_i \bar{m}_i h_i \right), \tag{65}$$

$$\rho u \frac{dY_i}{dx} + \frac{d\mathrm{J}_i^m}{dx} = \dot{\omega}_i \bar{m}_i, \quad i = 1, \ldots, N-1. \tag{66}$$

Equations (64)–(66) describe the steadily propagating laminar premixed flame, and the appropriate set of boundary conditions is

$$x = 0: \qquad T = T_o, \quad Y_i + \frac{\mathrm{J}_i^m}{\rho u} = Y_{io}, \quad i = 1, \ldots, N-1, \tag{67}$$

$$x \to \infty: \qquad \frac{dT}{dx} \to 0, \quad \frac{dY_i}{dx} \to 0, \quad i = 1, \ldots, N-1, \tag{68}$$

$$x = x_f: \qquad T = T_f, \tag{69}$$

where $x_f$ is a specified spatial point and $T_f$ is the specified temperature at that location.[7] A solution for this boundary value problem, Eqs. (64)–(66) with the boundary conditions Eqs. (67)–(69), can be obtained using `PREMIX`.[10]

Here, an adiabatic steady one-dimensional laminar premixed flame freely propagating in a stoichiometric hydrogen–air mixture at $p = 1\ atm$ is considered. The unburned mixture's temperature is $T_u = 800\ K$, the

specified temperature is assigned at $x_f = 2.30\ cm$ as $T_f = 900\ K$. Using a grid that has been adaptively refined to control the error and capture regions of steep gradient, a fully resolved steady species profile is obtained and presented in Fig. 6.

To numerically obtain all the length scales inherent in this system, the spatial eigenvalue spectrum of the system's governing equations is calculated. The robust method developed by Al-Khateeb *et al.*[1,2] to calculate the length scales is employed. As a result, the local length scales $\ell_i$ are predicted throughout the domain, Fig. 7. The multi-scale nature of the problem and the length scales over which the species evolve are shown. There are $2N - \mathsf{L} = 15$ length scales in the spectrum; this almost twice the number of time scales for the spatially homogeneous version. It would be exactly twice if element conservation were not a feature of this system. Extrapolating our analysis of the simple systems, we speculate for large domain lengths that many of these length scales in the spectrum will become irrelevant. The finest length scale and the largest length scale for this system vary from $7.60 \times 10^{-4}\ cm$ and $1.62 \times 10^{7}\ cm$ in the preheat zone to $2.41 \times 10^{-4}\ cm$ and $2.62 \times 10^{0}\ cm$ in the hot far-field region, respectively. The spatial stiffness in the hot region is $\mathcal{S}_x \sim \mathcal{O}(10^4)$.

### IV.C. Spatio-temporal spectrum

We next study the time spectrum of a reacting flow system. In principle, we would perturb the steady laminar flame structure of the previous section. However, this presents overwhelming computational demands in solving for eigenvalues of very large matrices.

As a useful alternative, we instead find the time scale spectrum associated with a system initially near a spatially homogenous chemical equilibrium state. This is certainly relevant for laminar flame structure, as it represents the hot end. A spatially homogeneous system at chemical equilibrium is subjected to a spatially inhomogeneous perturbation, and its spatio-temporal response is predicted. To achieve this, the equations are most conveniently posed as a set of $2N + 2$ partial differential algebraic equations (PDAEs) in terms of $2N + 2$ state variables $\mathbf{z}$, composed of species mass fraction $Y_i$, species mass flux $\mathrm{J}_i^m$, mixture specific enthalpy $h$, and Fourier heat flux q. This system, in a compact representation, is

$$\mathbf{A}(\mathbf{z}) \cdot \frac{\partial \mathbf{z}}{\partial t} + \mathbf{B}(\mathbf{z}) \cdot \frac{\partial \mathbf{z}}{\partial x} = \mathbf{f}(\mathbf{z}). \tag{70}$$

When $\mathbf{z} = \mathbf{z}^e$, a constant vector, the system is in its equilibrium state, such that $\mathbf{f}(\mathbf{z}^e) = \mathbf{0}$. At this state, $\mathbf{A}(\mathbf{z})$, $\mathbf{B}(\mathbf{z})$ take on constant values, $\mathbf{A}(\mathbf{z}^e) \equiv \mathbf{A}^e$, $\mathbf{B}(\mathbf{z}^e) \equiv \mathbf{B}^e$. We next define perturbations from the equilibrium state as $\mathbf{z}' \equiv \mathbf{z} - \mathbf{z}^e$. We next eliminate $\mathbf{z}$ in favor of $\mathbf{z}'$ and linearize $\mathbf{f}$ about $\mathbf{z}^e$ in Eq. (70) to obtain

$$\mathbf{A}^e \cdot \frac{\partial \mathbf{z}'}{\partial t} + \mathbf{B}^e \cdot \frac{\partial \mathbf{z}'}{\partial x} = \mathbf{J}^e \cdot \mathbf{z}'. \tag{71}$$

Here the constant Jacobian matrix $\mathbf{J}^e$ has been defined as

$$\mathbf{J}^e = \left.\frac{\partial \mathbf{f}}{\partial \mathbf{z}}\right|_{\mathbf{z}=\mathbf{z}^e}. \tag{72}$$

#### *IV.C.1. Continuous spectrum*

The continuous spectrum could be studied by assuming solutions of the form $\mathbf{z}'(x,t) = \mathbf{Z}(t)\exp(\mathbb{i}kx)$. We would arrive at a complicated generalized eigenvalue problem of finite dimension. This is challenging and will be examined in future work.

#### *IV.C.2. Discrete spectrum*

Even more challenging is the calculation of the discrete spectrum over a finite domain, which is again deferred to the future.

#### *IV.C.3. Spatially discretized spectrum*

We instead address the problem via spatial discretization of the spatial derivative operators. Equation (71) is spatially discretized using a second order finite difference approximation on a spatially uniform grid. Then,

the resulting equations are cast as a standard dynamical system of the form

$$\boldsymbol{\mathcal{A}}^e \cdot \frac{d\boldsymbol{\mathcal{Z}}}{dt} = (\boldsymbol{\mathcal{J}}^e - \boldsymbol{\mathcal{B}}^e) \cdot \boldsymbol{\mathcal{Z}}, \tag{73}$$

where $\boldsymbol{\mathcal{A}}^e$ and $\boldsymbol{\mathcal{J}}^e - \boldsymbol{\mathcal{B}}^e$ are matrices of dimensions $2\mathcal{N}(N+1) \times 2\mathcal{N}(N+1)$, and $\boldsymbol{\mathcal{Z}}$ is the set of state variables. Here $\boldsymbol{\mathcal{A}}^e$ is singular. This dynamical system is similar to the dynamical system studied in Sec. III. The generalized eigenvalues and the associated generalized eigenvectors of this dynamical system can be calculated, where the system's time scales are given by the reciprocal of its generalized eigenvlaues.

For the system resulting from perturbing the chemical equilibrium state of the one-dimensional laminar premixed hydrogen–air flame, the time scale spectrum is presented in Fig. 8, where the modified wavelength is defined by Eq. (53). Figure 8 clearly shows that the time scales associated with long wavelength modes match with the chemical time scales shown in Fig 5; they are dictated by reaction. Moreover, the diffusion effect starts to appear through the slowest time scales associated with small wavelength modes.

In Fig. 9, the system's times scales associated with the fundamental modes are tracked as we change the system's length. For large $L$, the reaction-advection-diffusion system's time scales and the reaction-only system's time scales are identical; compare Fig. 5 with Fig. 9 at large $L$. However, for $L/\pi \sim 10^{-1}$ $cm$ the effect of diffusion can be noted; it increases monotonically as $L$ decreases. Also, the balance between reaction and diffusion is clear: short wavelength modes are dominated by diffusion, and large wavelength modes are dominated by reaction. Furthermore, the effect of adopting non-uniform diffusion coefficients, the $D_{ij}$ in Eqs. (58), is noted in the diffusion dominated region, $L \leq 10^{-2}$ $cm$. One would expect $\tau \sim L^2/D_{ij}$, and thus on the log-log scale, $\ln \tau \sim 2 \ln L - \ln D_{ij}$, so that the slope of each should be the same, but the intercept is different for each $D_{ij}$. It is obvious that in the diffusion-dominated region, there is a two decade drop in $\tau$ for every one decade drop in $L$, consistent with our estimate.

It is clear from Figs. 8–9 that the branch associated with the slowest chemical time scales starts to become influenced by diffusion before branches associated with the faster chemical time scales; the turning point for the fastest chemical time scale branch is $L/\pi \sim 10^{-3}$ $cm$ and for the slowest chemical time scale branch is $L/\pi \sim 10^{-1}$ $cm$.

Now we can also try to estimate the turning points by a formula similar to Eq. (8). This is subject to greater error because we actually have a multicomponent diffusion process, coupled with diffusion of energy as well. Let us crudely estimate the diffusion coefficient as $D_{mix}$ and take it to be the largest of either the mixture mass diffusion coefficient or the energy diffusion coefficient. Our computational prediction gives $D_{mix} = 11$ $cm^2/s$, which arises from energy diffusion. Let us estimate the most rapid reaction rate as the reciprocal of the fastest reaction time constant, $a_f = 1/(8.3 \times 10^{-9}\ s) = 1.2 \times 10^8\ 1/s$ and likewise for the slowest reaction rate, $a_s = 1/(1.4 \times 10^{-4}\ s) = 7.1 \times 10^3\ 1/s$. Then we estimate the turning points for fast and slow reactions to be

$$\ell_f = \sqrt{\frac{D_{mix}}{a_f}} = 3 \times 10^{-4}\ cm, \tag{74a}$$

$$\ell_s = \sqrt{\frac{D_{mix}}{a_s}} = 5 \times 10^{-2}\ cm. \tag{74b}$$

Both of these estimates under-predict the turning points by a factor around two, and this is evident in Fig. 9. Interestingly, the simple estimate predicts the finest length scale shown by spatial eigenvalue analysis quite well. Reasons for the discrepancies are unclear, but could be related to the approximations involved such as the use of mixture properties in the estimates.

However, the location of the turning point for the slowest time scale, where the reaction-diffusion balance exists, is higher than our prediction in Sec. IV.B for the hydrogen–air flame. This may be due to the full laminar flame being composed of Fourier modes of smaller wavelengths which have more demanding time constants.

## V. Conclusion

The time scale spectrum of a one-dimensional atmospheric-pressure hydrogen–air system was calculated via conducting a generalized eigenvalue analysis. It was shown that when the reaction zone structure is resolved, the small wavelength modes critical in the thin reaction zone structures induced by fast reaction

have associated with them time scales which are dictated by a balance between reaction and diffusion. Moreover, for this time spectrum, one can say that: 1) short wavelength modes have very fast time scales which are dominated by diffusion, 2) modes which have wavelengths ranging from the finest combustion length scale to the coarsest combustion length scale have time scales which are dictated by a combination of reaction and diffusion effects, and 3) modes which have coarse wavelengths have time scales which are reaction-dominated.

The implications for the very fine length and time scales necessary to claim a resolved simulation, *i.e.* a Direct Numerical Simulation (DNS), of a combustion process with realistic kinetics and diffusion are obvious.

## Acknowledgments

The authors recognize the support of the National Science Foundation (NSF) under $CBET$-0650843, and the Center for Applied Mathematics at University of Notre Dame (CAM).

## References

[1]Al-Khateeb, A. N., Powers, J. M., and Paolucci, S., "On the Necessary Grid Resolution for Verified Calculation of Premixed Laminar Flames," *Communications in Computational Physics* (to appear).

[2]Al-Khateeb, A. N. and Powers, J. M., "Verified Computations of Laminar Premixed Flames," AIAA 2007-0381, Reno, NV, 2007.

[3]Golub, G. H. and Van Loan C. F., *Matrix Computations*, John Hopkins University Press, Baltimore, MD, 1983.

[4]Williams, F. A, *Combustion Theory*, Addison-Wesley, Redwood City, CA, 1985.

[5]Miller, J. A., Mitchell, R. E., Smooke, M. D., and Kee, R. J., "Toward a Comprehensive Chemical Kinetic Mechanism for the Oxidation of Acetylene: Comparison of Model Predictions with Results from Flame and Shock Tube Experiments," *Proceedings of the Combustion Institute*, Vol. 19, No. 1, 1982, pp. 181-196.

[6]Warnatz, J., Maas, U., and Dibble, R. W., *Combustion: Physical and Chemical Fundamentals, Modeling and Simulation, Experiments, Pollutant Formation*, Springer-Verlag, Berlin, Germany, 1996.

[7]Kee, R. J., Coltrin, M. E., and Glarborg, P., *Chemically Reactive Flow: Theory and Practice*, John Wiley & Sons, Hoboken, NJ, 2003.

[8]Smooke, M. D., Miller, J. A., and Kee, R. J., "Determination of Adiabatic Flame Speeds by Boundary Value Methods," *Combustion Science and Technology*, Vol. 34, No. 1-6, 1983, pp. 79-90.

[9]Hirschfelder, J. O., Curtiss, C. F., and Campbell, D. E., "The Theory of Flame Propagation. IV," *Journal of Physical Chemistry*, Vol. 57, No. 4, 1953, pp. 403-414.

[10]Kee, R. J., Grcar, J. F., Smooke, M. D., and Miller, J. A., "A Fortran Program for Modeling Steady Laminar One Dimensional Premixed Flames," Sandia National Labs., Rept. SAND85-8240, Livermore, CA, 1992.

**Table 1. Hydrogen–air detailed kinetics mechanism.**

| $j$ | Reaction | $A_j$ $\left[(mol/cm^3)^{1-\sum_{i=1}^{N}\nu'_{ij}}/s/K^{\beta_j}\right]$ | $\beta_j$ | $E_j$ $[cal/mol]$ |
|---|---|---|---|---|
| 1 | $H_2 + O_2 \rightleftharpoons OH + OH$ | $1.70 \times 10^{13}$ | 0.0 | 47780 |
| 2 | $OH + H_2 \rightleftharpoons H_2O + H$ | $1.17 \times 10^{9}$ | 1.3 | 3626 |
| 3 | $H + O_2 \rightleftharpoons OH + O$ | $5.13 \times 10^{16}$ | $-0.816$ | 16507 |
| 4 | $O + H_2 \rightleftharpoons OH + H$ | $1.80 \times 10^{10}$ | 1.0 | 8826 |
| 5 | $H + O_2 + M \rightleftharpoons HO_2 + M^{\mathrm{a}}$ | $2.10 \times 10^{18}$ | $-1.0$ | 0 |
| 6 | $H + O_2 + O_2 \rightleftharpoons HO_2 + O_2$ | $6.70 \times 10^{19}$ | $-1.42$ | 0 |
| 7 | $H + O_2 + N_2 \rightleftharpoons HO_2 + N_2$ | $6.70 \times 10^{19}$ | $-1.42$ | 0 |
| 8 | $OH + HO_2 \rightleftharpoons H_2O + O_2$ | $5.00 \times 10^{13}$ | 0.0 | 1000 |
| 9 | $H + HO_2 \rightleftharpoons OH + OH$ | $2.50 \times 10^{14}$ | 0.0 | 1900 |
| 10 | $O + HO_2 \rightleftharpoons O_2 + OH$ | $4.80 \times 10^{13}$ | 0.0 | 1000 |
| 11 | $OH + OH \rightleftharpoons O + H_2O$ | $6.00 \times 10^{8}$ | 1.3 | 0 |
| 12 | $H_2 + M \rightleftharpoons H + H + M^{\mathrm{b}}$ | $2.23 \times 10^{12}$ | 0.5 | 92600 |
| 13 | $O_2 + M \rightleftharpoons O + O + M$ | $1.85 \times 10^{11}$ | 0.5 | 95560 |
| 14 | $H + OH + M \rightleftharpoons H_2O + M^{\mathrm{c}}$ | $7.50 \times 10^{23}$ | $-2.6$ | 0 |
| 15 | $H + HO_2 \rightleftharpoons H_2 + O_2$ | $2.50 \times 10^{13}$ | 0.0 | 700 |
| 16 | $HO_2 + HO_2 \rightleftharpoons H_2O_2 + O_2$ | $2.00 \times 10^{12}$ | 0.0 | 0 |
| 17 | $H_2O_2 + M \rightleftharpoons OH + OH + M$ | $1.30 \times 10^{17}$ | 0.0 | 45500 |
| 18 | $H_2O_2 + H \rightleftharpoons HO_2 + H_2$ | $1.60 \times 10^{12}$ | 0.0 | 3800 |
| 19 | $H_2O_2 + OH \rightleftharpoons H_2O + HO_2$ | $1.00 \times 10^{13}$ | 0.0 | 1800 |

The non-unity third body collision efficiency coefficients are:

[a] for reaction 5, $\alpha_{H_2} = 3.3, \alpha_{H_2O} = 21$.

[b] for reaction 12, $\alpha_{H_2} = 3, \alpha_{H_2O} = 6, \alpha_H = 2$.

[c] for reaction 14, $\alpha_{H_2O} = 20$.

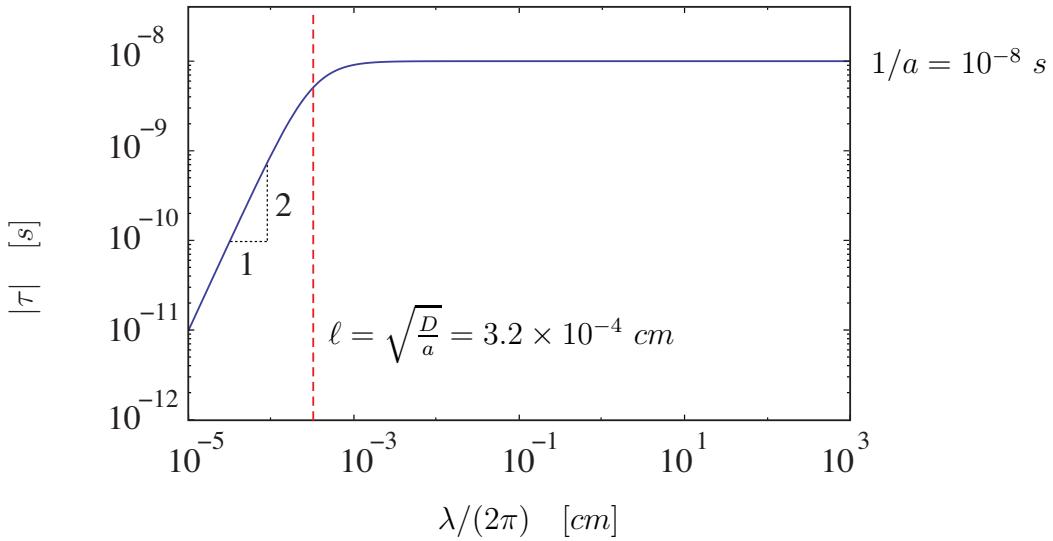


**Figure 1. Time scale spectrum for the versus wavelength for the simple one species reaction-advection-diffusion system;** $a = 10^8$ $1/s$, $D = 10^1$ $cm^2/s$, $u = 10^2$ $cm/s$.

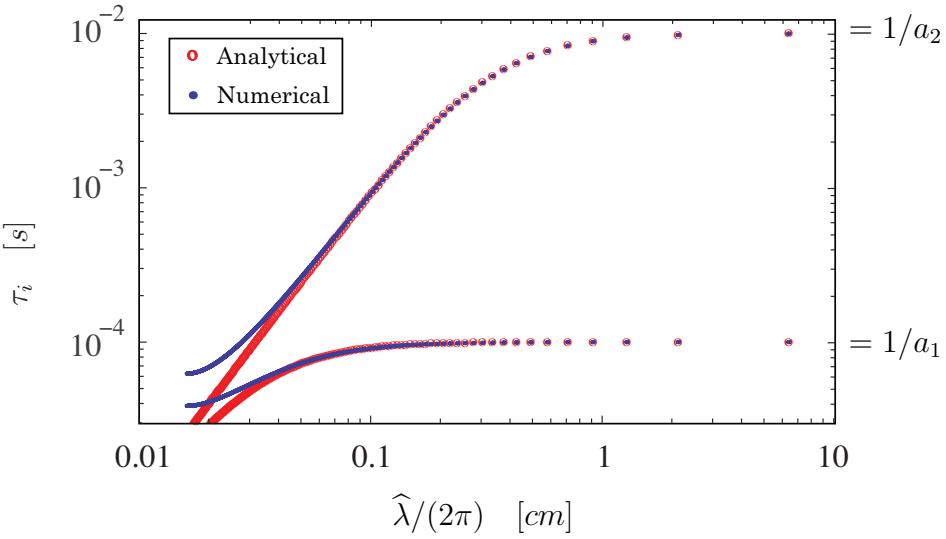


**Figure 2. Time scale spectrum versus the modified wavelength for the simple two species reaction-diffusion system,** $L = 10^1\ cm$, $\Delta x = 7.5 \times 10^{-3}\ cm$, $D = 10^1\ cm^2/s$, $a_1 = 10^4\ s^{-1}$, **and** $a_2 = 10^2\ s^{-1}$.

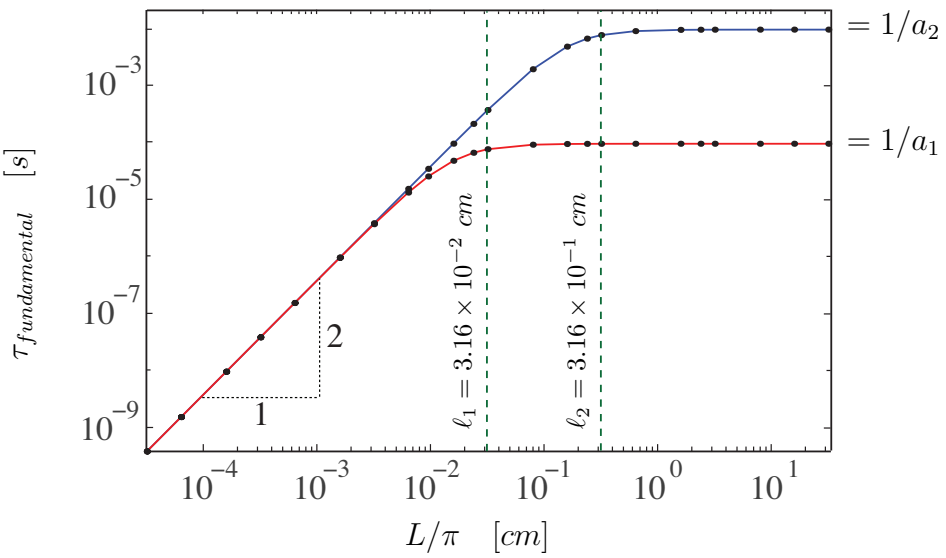


**Figure 3. Time scales associated with the fundamental modes versus the length,** $L/\pi$, **for the simple two species reaction-diffusion system.**

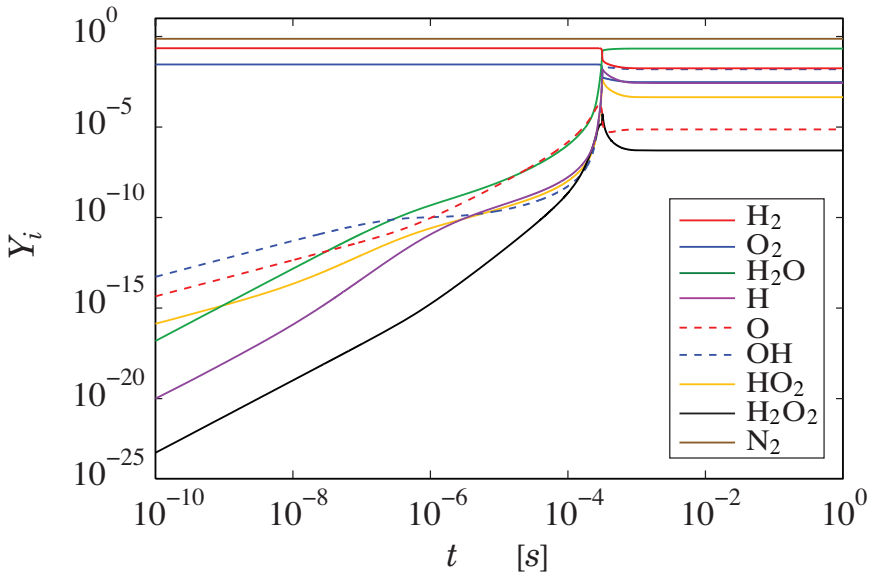


**Figure 4. Time evolution of species mass fractions for the spatially homogeneous stoichiometric hydrogen–air system, $T^* = 1000\ K$, $p = 1\ atm$.**

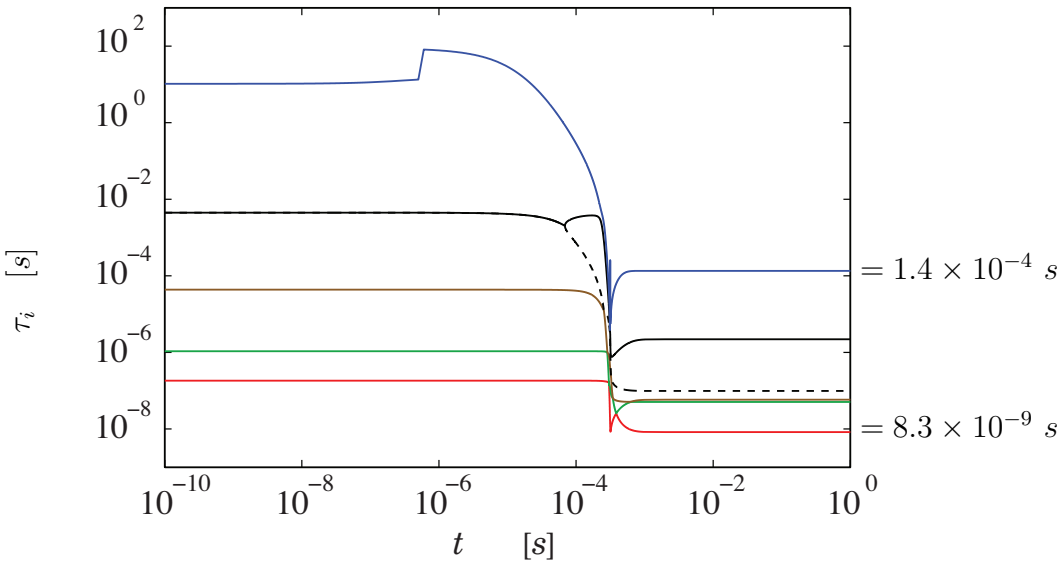


**Figure 5. Time scale spectrum over which a spatially homogenous stoichiometric hydrogen–air reactive system evolves, $T^* = 1000\ K$, $p = 1\ atm$.**

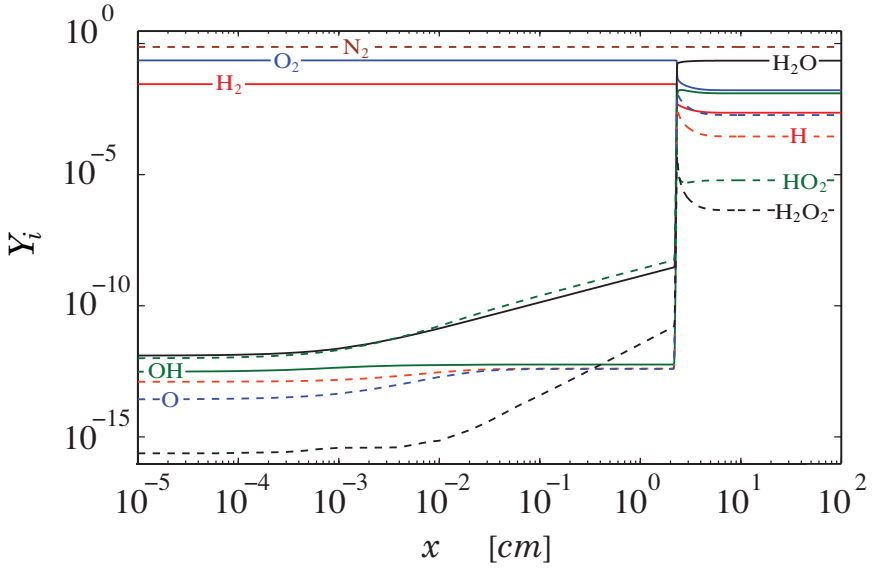


**Figure 6. Species mass fraction versus distance for a steady stoichiometric hydrogen–air flame,** $T_u = 800\ K, p = 1\ atm$.

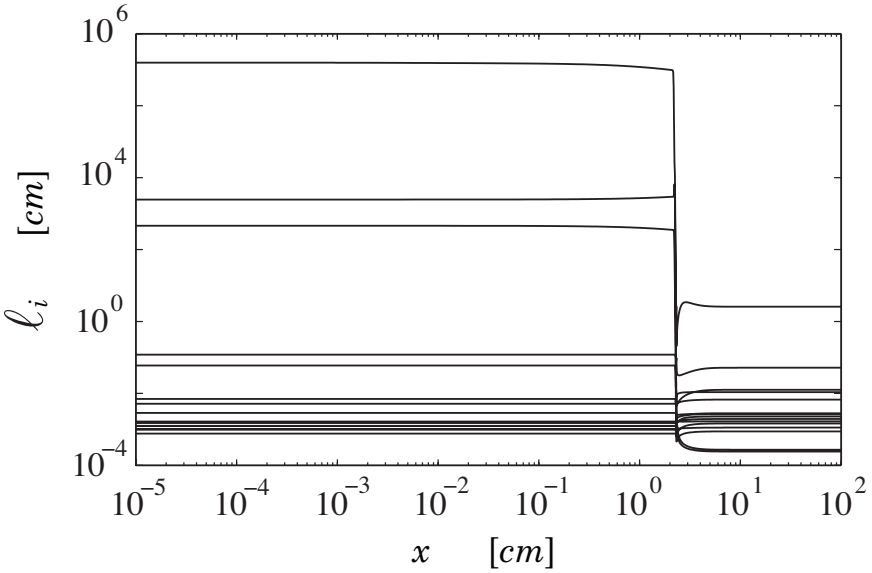


**Figure 7. Length scales over which a steady stoichiometric hydrogen–air flame evolves versus distance,** $T_u = 800\ K, p = 1\ atm$.

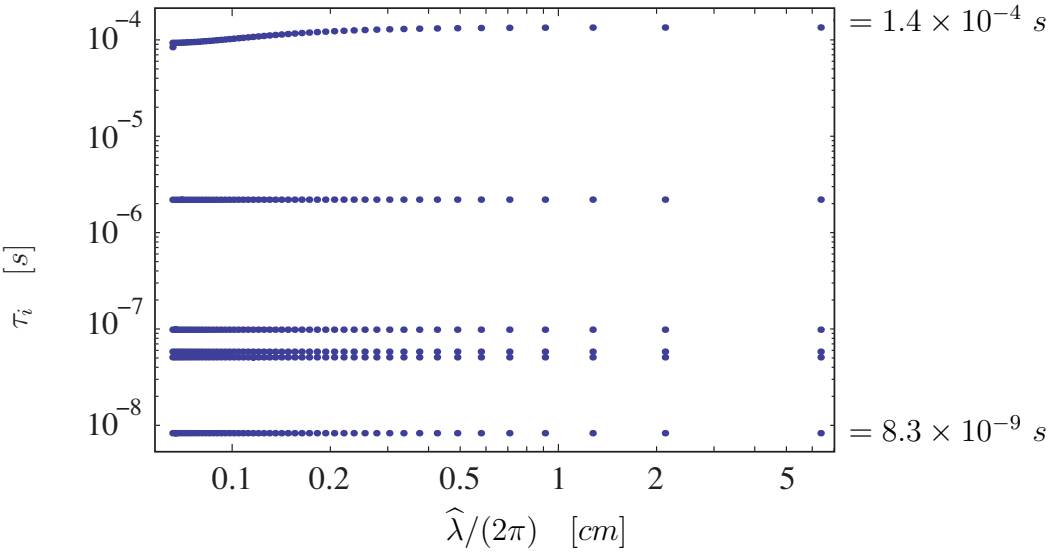


**Figure 8. Time scale spectrum for the hydrogen–air reaction-advection-diffusion system versus the modified wavelength;** $L = 10^1\ cm, \Delta x = 1 \times 10^{-2}\ cm$.

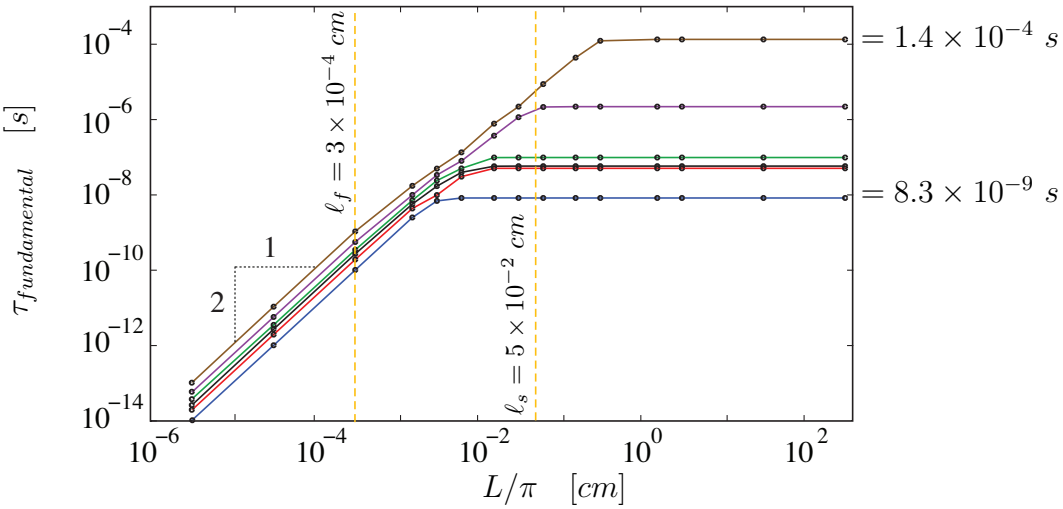


**Figure 9. Time scales associated with the fundamental modes for the hydrogen–air reaction-advection-diffusion system versus the length** $L/\pi$.